

---

---

# Log Normal Distribution of Cellular Uptake of Radioactivity: Implications for Biologic Responses to Radiopharmaceuticals

Prasad V.S.V. Neti and Roger W. Howell

*Division of Radiation Research, Department of Radiology, New Jersey Medical School, University of Medicine and Dentistry of New Jersey, Newark, New Jersey*

---

It is widely recognized that radiopharmaceuticals are generally distributed nonuniformly in tissues. Such nonuniformities are observed over the entire range of spatial levels, ranging from organ to subcellular levels. The implications of nonuniform distributions of radioactivity for dosimetry, and ultimately for the biologic response of tissues containing radioactivity, have been investigated extensively. However, there is a paucity of experimental data on the distribution of cellular activity within a population of cells. In the present study, the distribution of activity per cell is experimentally determined and its implications for predicting biologic response are examined. **Methods:** Chinese hamster V79 cells were exposed to different concentrations of  $^{210}\text{Po}$ -citrate. The radiolabeled cells were washed, seeded into culture dishes or glass slides, covered with photographic emulsion, and stored in an opaque container. Subsequently, the emulsion was developed, thereby resulting in observable  $\alpha$ -particle tracks that were scored. **Results:** The distribution of activity per cell was found to be well described by a log normal distribution function. Theoretic modeling of cell survival as a function of mean activity per cell showed that survival curves differed substantially when the activity per cell was log normally distributed versus when it was assumed conventionally that every cell in the population contained the mean activity. **Conclusion:** The present study provides experimental evidence of log normal cellular uptake of radioactivity. Theoretic calculations show that a log normal distribution of cellular activity can have a substantial impact on modeling the biologic response of cell populations.

**Key Words:** log normal distribution;  $^{210}\text{Po}$ ; autoradiography;  $\alpha$ -particle; cellular dosimetry

**J Nucl Med 2006; 47:1049–1058**

---

**I**t is widely recognized that radiopharmaceuticals are generally distributed nonuniformly in tissues. Such nonuniformities are observed over the entire range of spatial levels, including organ, suborgan, multicellular, cellular, and subcellular levels (1,2). Their implications for dosimetry, and

ultimately for the biologic response of tissues containing radioactivity, have been investigated extensively. Nonuniform distributions of radioactivity have the greatest impact on dose distributions produced by radionuclides that emit short-range radiations, such as  $\alpha$ -particles and Auger electrons (3). Accordingly, considerable effort has been devoted to the dosimetric consequences of microscopic nonuniformities of these radionuclides.

A generalized microdosimetry framework was developed for internal sources that has served as the starting point for many subsequent investigations (4). For lack of available experimental data, it was assumed that radionuclides were distributed randomly with a Poisson distribution and elegant microdosimetric spectra were calculated for nonuniform distributions of radioactivity (4). Tisljar-Lentulis et al. calculated specific energies deposited by  $^{239}\text{Pu}$  and  $^{131}\text{I}$  using a theoretic model consisting of spheric cells in closely packed geometry (5). The dependence of the distribution of specific energy on specific activity (e.g., activity per cell) was examined. These, and other, studies (6) paved the way for a variety of analyses that examined the impact of microdosimetry on cell survival curves. These studies were prompted in part by the observation of nonlinear survival curves (7). Humm and Chin found that if the radioactivity was distributed uniformly among all of the cells, a monoexponential survival curve resulted (8). However, when the radioactivity was restricted to a fraction of the cell population, 2-component exponential survival curves emerged. This type of survival curve was also observed by others when cells were targeted with  $\alpha$ -emitters (9,10). Their results suggest that not all cells were labeled uniformly with radioactivity. Roeske and Stinchcomb used analytic approaches to calculate microdosimetry spectra for cellularly localized  $\alpha$ -particle emitters to evaluate cell survival fractions (11). They found good agreement between theory and experimental monoexponential survival curves. Charlton and Turner examined the impact of  $\alpha$ -particle chord lengths on cell survival (12). Akabani and Zalutsky used histologic images to measure chord-length frequency distributions between source and target points for  $^{211}\text{At}$  in bone marrow (13). When applied to the survival of red bone

---

Received Oct. 3, 2005; revision accepted Mar. 6, 2006.  
For correspondence contact: Roger W. Howell, PhD, Department of Radiology, MSB F-451, New Jersey Medical School, UMDNJ, 185 S. Orange Ave., Newark, NJ 07103.  
E-mail: rhowell@umdnj.edu

marrow cells, their approach predicted monoexponential survival curves (13).

These microdosimetry studies generally assumed that radioactivity was distributed nonuniformly; however, it was assumed that the activity per labeled cell was the same. Cellular and multicellular approaches have made this assumption as well (14,15). In the present study, the distribution of activity per cell is experimentally determined in a culture of cells labeled with the radiochemical  $^{210}\text{Po}$ -citrate. These data are then used to examine the effect of activity distribution on cell survival.

## MATERIALS AND METHODS

### Overview

The distribution of radioactivity in tissues has been measured extensively using autoradiography.  $\alpha$ -Particles produce straight, dense tracks that are readily observed (16). Autoradiography has been used to quantify activity distributions (13,17–20). In the present study, autoradiography is used to measure the distribution of activity among a population of cultured cells that were labeled with  $^{210}\text{Po}$ -citrate. It is important to note that the cells in this study were radiolabeled while in suspension culture so that each cell was uniformly exposed to the radiochemical—that is, measured differences in cellular uptake of radioactivity within a given population could not be attributed to differences in extracellular activity concentration.

### Cell Line

Chinese hamster V79 lung fibroblasts were used in the present study. The different minimum essential media (MEMA, MEMB, and wash MEMA) and culturing conditions were described in detail in a previous publication (21). The plating efficiency was typically about 60%. All media and supplements used in this study were from Life Technologies. Cells were maintained in Falcon (Becton-Dickinson) 225-cm<sup>2</sup> sterile tissue culture flasks at 37°C in a humidified atmosphere with 5% CO<sub>2</sub> and 95% air and subcultured twice weekly or as required on reaching 80%–90% confluence. The cell line was tested to be free of *Mycoplasma*.

### Radiochemical

PoCl<sub>4</sub> in 2 mol/L HCl was obtained at a concentration of 74 MBq/mL from Isotope Products.  $^{210}\text{Po}$ -citrate was prepared by mixing PoCl<sub>4</sub> solution with 1 mol/L sodium citrate in the ratio of 1:7 (final pH 5.8). This was diluted with MEMB in the ratio of 1:19 (final pH 6.9).

### Radiolabeling with $^{210}\text{Po}$ -Citrate

V79 cells were grown as monolayers in 225-cm<sup>2</sup> Falcon flasks, washed with 20 mL of phosphate-buffered saline, trypsinized with 0.05% trypsin/0.53 mmol/L ethylenediaminetetraacetic acid, and suspended at  $4 \times 10^6$  cells per mL in MEMB. Aliquots of 1 mL were placed in sterile 17 × 100 mm Falcon polypropylene round-bottom culture tubes and placed on a rocker-roller (Fisher Scientific) for 3–4 h at 37°C in an atmosphere of 95% air and 5% CO<sub>2</sub>. After this conditioning period, 1 mL of MEMB containing  $^{210}\text{Po}$ -citrate was added to arrive at a final concentration of 0–67 kBq/mL (pH 6.9–7.0). The tubes were returned to a rocker-roller at 37°C in 95% air and 5% CO<sub>2</sub>. After 30 min, the cells were washed 3 times with wash MEMA, resuspended in 5 mL of MEMA, and passed 5 times through a 21-gauge needle. The cell concentration

in each tube was determined with a calibrated Coulter model ZM (Coulter Electronics). Aliquots (500  $\mu\text{L}$ ) of the cell suspension were transferred to vials containing 5 mL Ecolume liquid scintillation cocktail (MP Biomedicals) and counted in a Beckman LS5000 liquid scintillation counter for  $^{210}\text{Po}$  activity, and the mean activity per cell  $\langle a_o \rangle$  was determined (counting efficiency, 50%). Aliquots of labeled cell suspension were also mixed 1:1 with 4% trypan blue solution (Fluka Chemie). These cells were loaded into a hemocytometer and viewed at 100 $\times$  magnification, and the number of live (trypan blue negative) and dead (trypan blue positive) cells was scored in about 3,000 cells. The percentage of dead cells in the populations labeled at 0–67 kBq/mL ranged from 3.0% to 3.1%.

### Autoradiography

After washing the cells, 20,000 cells were seeded in triplicate into Falcon 35 mm × 10 mm culture dishes (Becton-Dickinson) containing 2 mL MEMA and then incubated. Three culture dishes were seeded with unlabeled control cells. Twenty-four hours after seeding, the dishes were washed 3 times with normal saline, fixed with 100% ethanol, and allowed to air dry (experiment A). Alternatively, 20,000 washed cells were immediately and gently smeared on a clean microscope slide that was then briefly passed over the flame of a Bunsen burner. These cells were not subjected to ethanol fixation (experiments B and C). The dishes were taken into a dark room, and a small volume of Kodak NTB emulsion that was sufficient to cover the bottom of the dish was applied. The dish was then tipped upside down at an angle and allowed to drain and dry. Slides were dipped in GE Amersham Hypercoat EM-1 emulsion, stood upright, and allowed to drain and dry for 10 min. The dishes or slides were then placed in black boxes containing predried Dry-Rite crystals (W.A. Hammond DRIERITE Co. Ltd.) to minimize the humidity, sealed with opaque tape, and maintained at 4°C to allow for accumulation of  $^{210}\text{Po}$  decays. Each box also contained one control dish or slide. The exposure times were varied depending on the desired track density. The emulsion was developed in Kodak D19 developer for 10 min. The dishes or slides were quickly rinsed with deionized water, and then a fixer solution was added for 5 min and removed. Upon drying, the resulting  $\alpha$ -particle tracks were observed under phase-contrast with an Olympus IX70 inverted microscope with 400 $\times$  magnification equipped with a digital camera. The number of tracks per cell was scored in the cells in each dish or slide. Only clearly visible tracks with a length greater than 2–3  $\mu\text{m}$  were scored. Cells with up to 9 tracks per cell were scored according to their specific number of tracks. Because of the uncertainties associated with counting large numbers of overlying tracks, cells with >9 tracks per cell were recorded as >9. The subcellular location of the decays (cytoplasm or nucleus) was scored accordingly for experiment A. No background tracks were visible in controls. The tracks were scored in 500–1,200 cells for each  $^{210}\text{Po}$ -citrate concentration and emulsion exposure time.

### Analysis of Track Data

Only datum where >20 cells were scored in a given category (e.g., 20 cells with 9 tracks/cell) were used in the analysis. This approach ensured that each datum was scored to within an uncertainty ( $\sqrt{n/n}$ ) of <20%. Because of this statistical constraint, and because cells with >9 tracks per cell could not be scored, any given dish or slide could provide the track distribution within only a limited range of tracks per cell. Therefore, datasets with

different exposure times were convolved to obtain a complete distribution of tracks per cell. This was done by decay correcting the data for each time point to the latest time point in the set and then normalizing the data using overlapping regions of the data. To shed more light on this process, consider the following example taken from our data where the cells were treated with 0.52 kBq/mL. After 7 d of decay accumulation, a maximum of 6 tracks was found in any given cell and many of the cells had no tracks. The remaining dishes or slides were maintained for a longer time (26 and 52 d) to accumulate additional decays with the aim of reducing the percentage of cells with zero tracks and increasing the number of cells with >6 tracks per cell. As expected, the number of zero-track cells was greatly reduced; however, the number of cells with an unscorable number of tracks per cell (>9) was substantial. The numbers of tracks per cell from the 7-d exposure data were decay corrected to 52 d (i.e.,  $N(t_1 \Rightarrow t_2) = (1 - \exp(-0.693 t_2/T_p)) / (1 - \exp(-0.693 t_1/T_p))$ ) and then normalized so that the percentage of cells from the 7-d decay-corrected data with >9 tracks was equal to the number of cells with >9 tracks in the 52-d data. The same approach was also used for the 26-d data. In this manner, a complete convolved track distribution for a 52-d exposure was obtained, with the 52-d data providing the distribution for the lower multiplicity of convolved tracks ( $0 \leq$  convolved tracks  $\leq 9$ ), the 7-d data providing the distribution of the higher multiplicity ( $11 \leq$  convolved tracks  $\leq 32$ ), and the 26-d data providing the distribution in the overlapping region ( $4 \leq$  convolved tracks  $\leq 15$ ).

### Determination of Activity Distribution Among the Cell Population

After exposing the emulsion for a time  $\tau$ , the number of tracks observed in a given cell at time  $\tau$  is  $N(\tau)$ , which is directly proportional to the cumulated activity in that cell  $\tilde{a}(\tau)$  according to:

$$N(\tau) = \eta \tilde{a}(\tau), \quad \text{Eq. 1}$$

where  $\eta$  is the track detection efficiency. The cumulated activity may be expressed as:

$$\tilde{a}(\tau) = \int_0^\tau a(t) dt = \int_0^\tau a_0 e^{-0.693 t/T_p} dt = 1.44 a_0 T_p \left(1 - e^{-0.693 \tau/T_p}\right), \quad \text{Eq. 2}$$

where  $a_0$  is the initial activity in that cell at  $t = 0$  and  $T_p$  is the physical half-life of the radionuclide ( $T_p = 138$  d for  $^{210}\text{Po}$ ). Thus, the track data can be used to obtain the initial activity in a given cell,  $a_0$ , by solving Equation 2 for  $a_0$  and substituting in  $\tilde{a}(\tau)$  from Equation 1:

$$a_0 = \frac{N(\tau)}{1.44 T_p \eta (1 - e^{-0.693 \tau/T_p})}. \quad \text{Eq. 3}$$

The track detection efficiency  $\eta$  can be obtained from the experimentally determined mean cellular activity  $\langle a_0 \rangle$  and the mean number of tracks per cell  $\langle N(\tau) \rangle$  in the cell population. Note the difference in notation for the activity in a given cell,  $a_0$ , and the mean activity in the cell population  $\langle a_0 \rangle$ :

$$\eta = \frac{\langle N(\tau) \rangle}{1.44 T_p \langle a_0 \rangle (1 - e^{-0.693 \tau/T_p})}. \quad \text{Eq. 4}$$

As described above,  $\langle a_0 \rangle$  was obtained experimentally by measuring activity in aliquots of labeled cell suspensions. The

quantity  $\langle N(\tau) \rangle$  must be obtained from the track distribution data. One possibility is to obtain  $\langle N(\tau) \rangle$  from discrete raw track data at a single exposure time. In this case, the data would be expected to follow a Poisson distribution. However, the breadth of the track distribution data from a single exposure time does not fully describe the entire distribution (Results). Therefore, it is essential to use the convolution process described above to completely define the distribution. The convolution process results in noninteger track values. Hence, the convolved track data are continuous and should be represented with a continuous function. Supporting this line of reasoning is that the activity distribution, which will be obtained from the convolved track distribution, is continuous. For  $^{210}\text{Po}$ -citrate, the convolved track distribution data are well represented by a log normal function of the form (22):

$$f(N) = \frac{g}{N\sigma} e^{-(\ln N - \mu_N)^2 / 2\sigma^2}, \quad N > 0 \quad \text{Eq. 5}$$

where  $N$  is the number of convolved tracks,  $\mu_N$  is the scale parameter for the convolved track distribution,  $\sigma$  is the shape parameter, and  $g$  is a constant. Mathematically, this distribution function has 4 raw moments and 3 central moments. Integration of these moments gives a variety of statistical quantities, including the arithmetic mean, variance, skewness, kurtosis, and coefficient of variation (CV) (<http://mathworld.wolfram.com/LogNormalDistribution.html>). The expectation value  $\langle N \rangle$  (also known as the arithmetic mean) is given by (22):

$$\langle N \rangle = e^{\mu_N + \sigma^2/2}. \quad \text{Eq. 6}$$

The remaining statistical quantities are provided in Equation 7 (22):

$$\left. \begin{aligned} \text{Variance} &= e^{2\mu_N + \sigma^2} (e^{\sigma^2} - 1) \\ \text{Median} &= e^{\mu_N} \\ \text{Mode} &= e^{\mu_N - \sigma^2} \\ \text{Skewness} &= (e^{\sigma^2} + 2) \sqrt{e^{\sigma^2} - 1} \\ \text{Kurtosis} &= e^{4\sigma^2} + 2e^{3\sigma^2} + 3e^{2\sigma^2} - 6 \\ \text{CV} &= \sqrt{e^{\sigma^2} - 1} \end{aligned} \right\} \quad \text{Eq. 7}$$

Because the cellular activity is directly proportional to the number of convolved tracks (Eq. 3), the distribution of activity per cell is also described by a log normal function. The mean initial cellular activity  $\langle a_0 \rangle$  and the statistical quantities for the log normal activity distribution can be obtained from Equations 6 and 7 by substituting  $\mu_a$  for  $\mu_N$ , where  $\mu_a$  is the scale parameter for the activity distribution. Accordingly,  $\langle a_0 \rangle$  is given by:

$$\langle a_0 \rangle = e^{\mu_a + \sigma^2/2}. \quad \text{Eq. 8}$$

The normalized *probability density function* for the initial cellular activity  $a_0$  can be written as:

$$f(a_0) = \frac{1}{a_0 \sigma \sqrt{2\pi}} e^{-(\ln a_0 - \mu_a)^2 / 2\sigma^2}, \quad a_0 > 0 \quad \text{Eq. 9}$$

This function satisfies several conditions, including  $\int_0^\infty f(a_0) da_0 = 1$  and  $\lim_{a_0 \rightarrow 0} f(a_0) = 0$ . The cumulative distribution function  $F(a_0)$  for the log normal distribution is:

$$F(a_0) = \int_0^{a_0} f(a_0) da_0 = \frac{1}{2} \left[ 1 + \operatorname{erf} \left( \frac{\ln a_0 - \mu_a}{\sigma\sqrt{2}} \right) \right], \quad \text{Eq. 10}$$

where  $\operatorname{erf}(x)$  is the error function. The  $\operatorname{erf}$  function follows the symmetry relation  $\operatorname{erf}(-x) = -\operatorname{erf}(x)$ . It should be noted that  $\lim_{a_0 \rightarrow \infty} F(a_0) = 1$ , which implies that the distribution is normalized.

The properties of the log normal function, coupled with Equation 3, dictate that the shape parameter  $\sigma$  for the activity distribution is the same as that for the convolved track distribution. However, the scale parameter  $\mu_a$  will be determined by the experimentally measured value of  $\langle a_0 \rangle$ . Solving Equation 8 for  $\mu_a$  yields the scale parameter for the log normal distribution of activity per cell for a given  $\langle a_0 \rangle$ :

$$\mu_a = \ln \langle a_0 \rangle - \sigma^2/2. \quad \text{Eq. 11}$$

It can be helpful to write the probability density function for the log normal distribution in terms of the experimentally determined  $\langle a_0 \rangle$  and the shape parameter  $\sigma$ . Substituting  $\mu_a$  from Equation 11 into Equation 9 yields:

$$f(a_0) = \frac{1}{a_0 \sigma \sqrt{2\pi}} e^{-\frac{(\ln a_0 - (\ln \langle a_0 \rangle - \sigma^2/2))^2}{2\sigma^2}}, \quad a_0 > 0 \quad \text{Eq. 12}$$

Thus, only the mean activity per cell  $\langle a_0 \rangle$  and the shape parameter  $\sigma$  are needed to describe the probability density function. If  $\langle a_0 \rangle$  is known experimentally, then only  $\sigma$  is required.

## RESULTS

### Mean Cellular Activity

As shown in Figure 1, measurements of activity in aliquots of radiolabeled cell suspensions revealed that  $\langle a_0 \rangle$  was linearly dependent on the extracellular concentration  $C$  of  $^{210}\text{Po}$ -citrate over the range of concentrations studied ( $\langle a_0 \rangle = kC$ ,  $k = 0.027 \pm 0.0012$  (mBq/cell)/(kBq/mL)). This value is similar to our earlier measurements of cellular

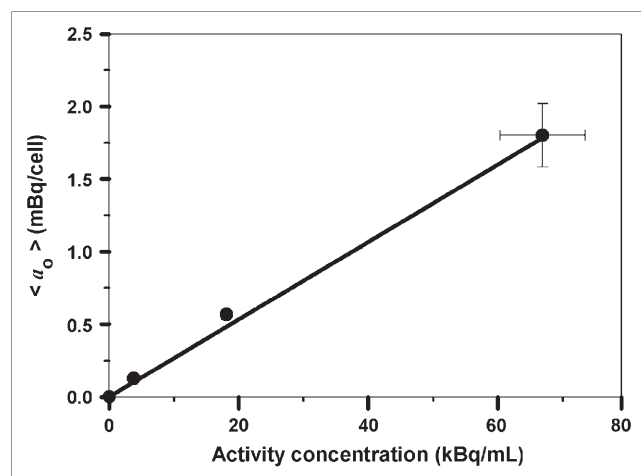


**FIGURE 1.** Initial mean cellular activity  $\langle a_0 \rangle$  as function of activity concentration  $C$  of  $^{210}\text{Po}$ -citrate in culture medium for representative experiment. Error bars represent SD of mean for 3 replicate measurements of  $\langle a_0 \rangle$  and  $C$ . Solid line represents linear least-squares fit of the data.

uptake of  $^{210}\text{Po}$ -citrate in this cell line (23). Measurements after radiolabeled cells were incubated for 24 h in culture medium revealed that  $\langle a_0 \rangle$  decreased by  $\sim 50\%$  of the initial value when cells were labeled at low concentrations of  $^{210}\text{Po}$ -citrate (3–4 kBq/mL), whereas no change was observed when cells were labeled at high concentrations (31–38 kBq/mL). Ethanol fixation of the cells, immediately after radiolabeling or after culturing the radiolabeled cells for 24 h, also reduced  $\langle a_0 \rangle$  by  $\sim 50\%$ .

### $\alpha$ -Particle Tracks

Figure 2 shows representative photographs of  $\alpha$ -particle tracks in V79 cells that were labeled with  $^{210}\text{Po}$ -citrate. Cells with 0, 1, 3, 5, 7, and a large number of tracks ( $>9$ ) are shown. The length of the track depends on its angle of trajectory. Given that the cell diameter of a V79 cell is about  $10 \mu\text{m}$ , it is apparent that the length of the long tracks in Figure 2 roughly correlates with the range of the  $^{210}\text{Po}$  5.3-MeV  $\alpha$ -particles in Kodak NTB emulsion, which is  $21.5 \mu\text{m}$  (24). This contrasts with their range of  $40 \mu\text{m}$  in water (25). Given the stringent scoring requirement of only counting tracks with lengths  $>2\text{--}3 \mu\text{m}$ , solid angle

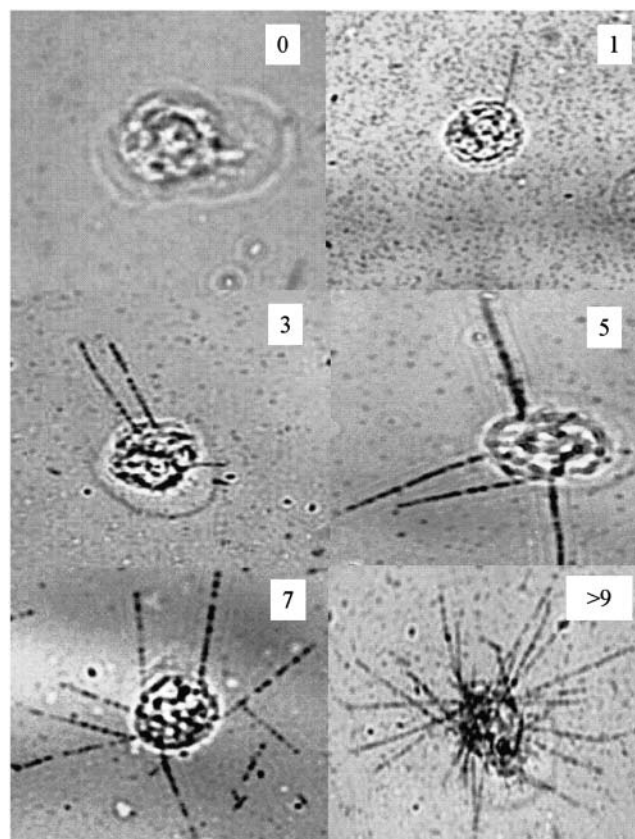


**FIGURE 2.** Autoradiographs of cells within a population exposed to culture medium containing 67 kBq/mL of  $^{210}\text{Po}$ -citrate. These images show cells with 0, 1, 3, 5, 7, and  $>9$   $\alpha$ -particle tracks, demonstrating wide variation in cellular uptake of  $^{210}\text{Po}$ -citrate.

arguments suggest that only about 10% of the decays will yield a scoreable track when the emulsion thickness is 1  $\mu\text{m}$ .

### Subcellular Distribution of Decay Sites

The subcellular compartment in which the radioactive decay took place (i.e., where the track was initiated) was scored for experiment A (7 d). About 35% of the intracellular radioactivity was in the cell nucleus and 65% in the cytoplasm when a single decay took place in the cell. When 2 decays occurred in the cell (2 in cytoplasm, or 2 in nucleus, or 1 in cytoplasm and 1 in nucleus), then 33% and 67% of them were in the cell nucleus and cytoplasm, respectively. These values correspond closely with earlier measurements (28% and 72%, respectively) that used a slightly different  $^{210}\text{Po}$ -citrate recipe ( $^{210}\text{Po}$  dissolved in 3N nitric acid), no fixation with ethanol, and subcellular fractionation techniques to isolate the cell nuclei (23).

### Distribution of $\alpha$ -Particle Tracks per Cell

Figure 3 shows the distribution of tracks per cell after cells were radiolabeled with  $^{210}\text{Po}$ -citrate. Figure 3A shows the data for experiment A. When the emulsion was developed after 7 d of exposure, a maximum of 6 tracks was counted in any given cell and many of the cells had no tracks ( $\sim 45\%$ ). When samples were developed 26 d after applying the emulsion, the number of zero tracks was  $\sim 10\%$ . The percentage of cells with zero tracks at 52 d ( $\sim 14\%$ ) was almost the same as for the 26-d data (Fig. 3A). Figures 3B and 3C show the track data for experiments B and C, respectively. The percentages of cells with zero tracks were somewhat lower in these datasets (3.4% and 3.3%, respectively). It is evident from the keys of Figures 3A–3C that the required exposure times shorten as  $\langle a_o \rangle$  increases.

As pointed out in the Materials and Methods, it is apparent from Figure 3 that any given set of discrete track data (e.g., 7, 26, or 52 d) can provide the distribution within only a limited region of tracks per cell. Accordingly, the data in Figures 3A–3C are convolved and presented in Figures 4A–4C. The zero track data were not included in the convolved data for the following reasons: (a) Many of the cells with zero tracks would eventually evolve into cells with tracks if the emulsions were exposed for longer periods of time, (b) the log normal distribution requires values  $> 0$ , and (c) trypan blue exclusion measurements indicate that about 3% of the cells—both control cells and labeled cells—were not viable, and these nonviable cells do not participate in the subsequent measurement of biologic endpoints such as colony-forming survival assays. These aspects are further discussed in both the Materials and Methods and the Discussion. A nonlinear least-squares fit to the data using the log normal function (Equation 5) was used. The fitted parameters ( $\mu_N$ ,  $\sigma$ ) and other statistical quantities for the convolved track distribution are given in Table 1. The goodness of the fits is evident from the curves in Figures 4A–4C and the  $R^2$  values in Table 1. The mean number of convolved tracks per cell  $\langle N \rangle$ , calculated using Equation 6, were 7.1, 6.9, and 6.7 for Figures 4A, 4B, and

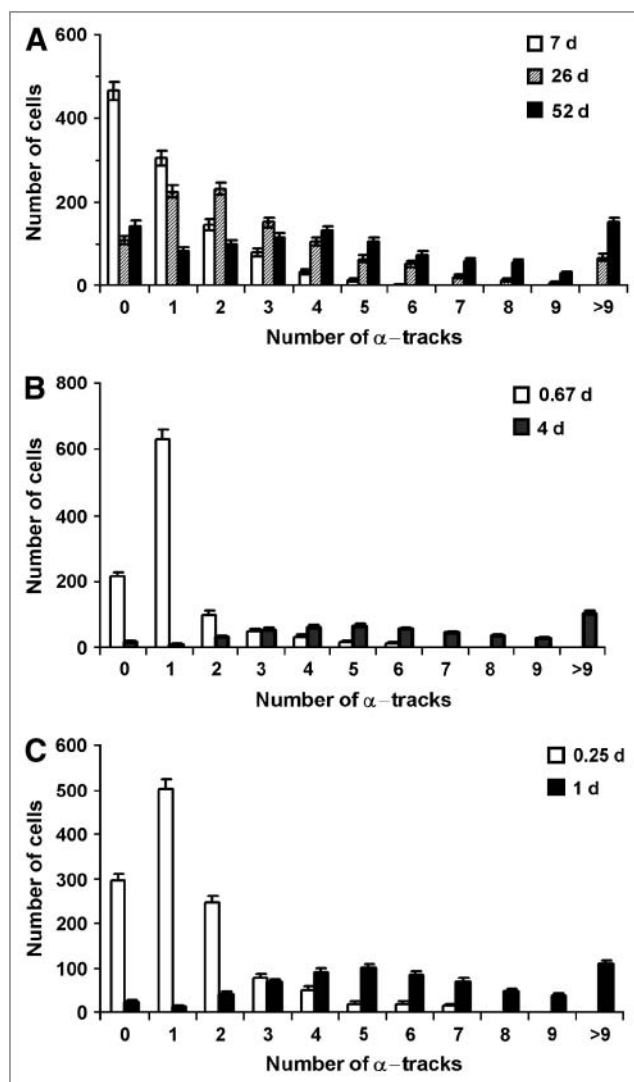


**FIGURE 3.** Distribution of  $\alpha$ -particle tracks in cells that were incubated in culture medium containing  $^{210}\text{Po}$ -citrate: 0.52 kBq/mL (A), 3.8 kBq/mL (B), 67 kBq/mL (C).  $\langle a_o \rangle$  was 0.054, 0.12, and 1.8 mBq per cell in A, B, and C, respectively. Decays were allowed to accumulate for different times, as indicated in the keys in A–C.

4C, respectively. These values of  $\langle N \rangle$ , along with the experimentally measured values of  $\langle a_o \rangle$  and the exposure time  $\tau$ , were substituted into Equation 4 to obtain track detection efficiencies ( $\eta$ ) of 3.3%, 16%, and 4.3% in each case, respectively. These are about the same as our rough estimates based on solid angle arguments. Finally, the initial activity per cell  $a_o$  corresponding to a given number of convolved tracks was calculated using Equation 3. These  $a_o$  data were used as the basis for defining the upper abscissae in Figures 4A–4C. As expected, least-squares fits to these activity data using Equation 5 (substituting  $N \rightarrow a_o$  and  $\mu_N \rightarrow \mu_a$ ) yielded the same shape parameters  $\sigma$ , but different values of the scale parameter. The fitted parameters  $\mu_a$  and  $\sigma$  are given in Table 2 along with the statistical quantities related to the activity distribution. Finally, it is

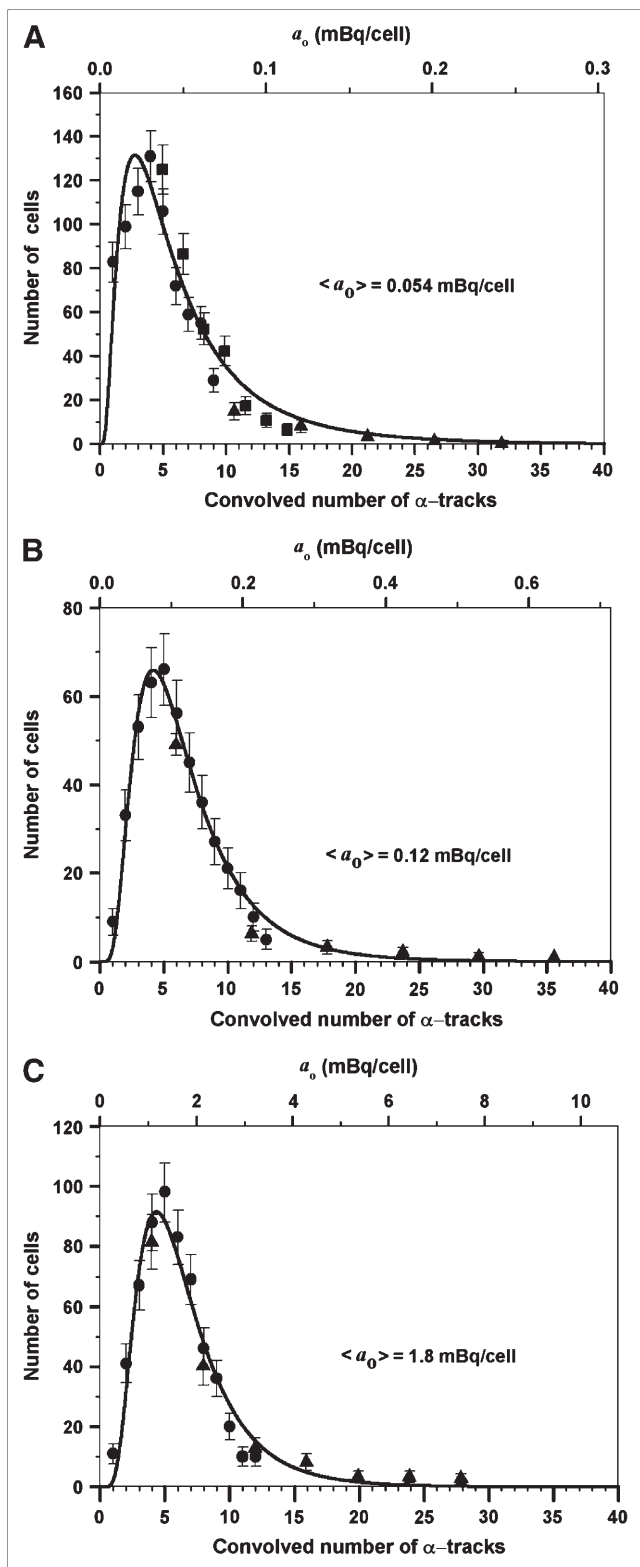


**FIGURE 4.** Distribution of convolved  $\alpha$ -particle tracks (lower abscissae) and initial cellular activity (upper abscissae) in cell populations having mean activity per cell  $\langle a_0 \rangle$  of 0.054 mBq per cell (A), 0.12 mBq per cell (B), and 1.8 mBq per cell (C).  $\alpha$ -Particle tracks are result of convolving the data shown in Figure 3. Data arising from different decay accumulation times are denoted with different symbols: (A) 52 d ( $\bullet$ ), 26 d ( $\blacksquare$ ), 7 d

( $\blacktriangle$ ); (B) 4 d ( $\bullet$ ), 0.67 d ( $\blacktriangle$ ); and (C) 1 d ( $\bullet$ ), 0.25 d ( $\blacktriangle$ ). The close correspondence of convolved data from different time points supports the accuracy of the convolution approach. Error bars represent SE. Cellular activity was calculated from track data using Equation 3. Curve represents least-squares fit of Equation 5 to convolved track data. Details regarding fitted parameters and corresponding statistical quantities are given in Table 1. Parameters related to cellular activity are given in Table 2.

interesting to note that fixing cells with ethanol does not substantially alter the shape of the distribution as evidenced by a comparison of Figure 4A (fixed) with Figures 4B and 4C (not fixed). The log normal probability density functions for the initial cellular activity  $a_0$ , defined by Equation 9 and the fitted parameters in Table 2, are depicted in Figure 5. Note that the normalization requirement inherently contained within Equation 9 results in a rescaling of the ordinate  $f(a_0)$  as one moves from low  $\langle a_0 \rangle$  (Fig. 5A) to high  $\langle a_0 \rangle$  (Fig. 5C). This can be understood more fully with the cumulative distribution function  $F(a_0)$  in Equation 10. In each case, the cumulative distribution function limits to a value of 1.

## DISCUSSION

Ultimately, it is desired to know the activity distribution at the cellular level among a large population of cells that have been labeled with a radiopharmaceutical. The number of tracks in a given cell is directly proportional to the cumulated activity, which, in turn, is directly proportional to cellular activity. Therefore, the distribution of tracks per cell can also be used to describe the distribution of activity per cell. The distribution of convolved tracks per cell represented by the data points shown in Figure 4 indicates that there is a wide variation in cellular uptake of  $^{210}\text{Po}$ -citrate despite the fact that these cells were suspended in the same extracellular concentration of the radiochemical. This variation in cellular activity can have a considerable impact on the biologic response of the cell population. Accordingly, it may be of considerable importance to quantify mathematically the distribution for subsequent use in predicting biologic response (26,27). In view of the trend of the data in Figure 4, a log normal function was selected to fit the data. No attempt was made to establish a biologic basis for this function and more complex distribution functions were not considered. Nevertheless, the log normal function provided a reasonable fit to the data with only 2 parameters—namely, the scale parameter  $\mu$  and the shape parameter  $\sigma$ . It is evident that the log normal distribution exhibits the desired property of nonnegativity despite the large skewness of the distribution. The motivation for using the log normal distribution rather than the normal (Gaussian) distribution is apparent in the present case and has been discussed in detail for many other scientific applications (27). In fact, log normal distributions are so prolific in biology (27) that one might almost anticipate such a distribution for cellular uptake of radioactivity.

**TABLE 1**  
Fitted Parameters and Statistical Quantities for Log Normal Convolved Track Distributions

| Parameter  | Value          |              |              |
|--|----------------|--------------|--------------|
|  | A              | B            | C            |
| Experiment   |                |              |              |
| Labeling concentration (kBq/mL)*                         | 0.52 ± 0.051   | 3.8 ± 0.36   | 67 ± 6.6     |
| Mean cellular activity <a <sub>o</sub> > (mBq/cell)*     | 0.054 ± 0.0037 | 0.12 ± 0.011 | 1.8 ± 0.22   |
| Maximum time of emulsion exposure (d)                    | 52             | 4            | 1            |
| Scale parameter (μ <sub>N</sub> ) <sup>†</sup>           | 1.6 ± 0.072    | 1.8 ± 0.027  | 1.8 ± 0.031  |
| Shape parameter (σ) <sup>†</sup>                         | 0.80 ± 0.056   | 0.59 ± 0.023 | 0.54 ± 0.029 |
| Goodness of fit (R <sup>2</sup> )                        | 0.92           | 0.98         | 0.97         |
| Arithmetic mean <N> (convolved tracks/cell) <sup>‡</sup> | 7.1 ± 0.63     | 6.9 ± 0.22   | 6.7 ± 0.25   |
| Median (convolved tracks/cell) <sup>‡</sup>              | 5.2 ± 0.37     | 5.8 ± 0.16   | 5.8 ± 0.18   |
| Mode (convolved tracks/cell) <sup>‡</sup>                | 2.7 ± 0.31     | 4.2 ± 0.16   | 4.3 ± 0.19   |
| Variance <sup>‡</sup>                                    | 45 ± 13        | 20 ± 2.3     | 15 ± 2.3     |
| Skewness <sup>‡</sup>                                    | 3.7 ± 0.51     | 2.2 ± 0.12   | 1.9 ± 0.14   |
| Kurtosis <sup>‡</sup>                                    | 34 ± 10        | 12 ± 1.2     | 10 ± 1.2     |
| Coefficient of variation (CV)                            | 0.94           | 0.64         | 0.58         |
| Cumulative probability for 1–9 tracks (%)                | 74             | 77           | 79           |
| Cumulative probability for 10–40 tracks (%)              | 20             | 18           | 15           |
| Cumulative probability for <1 track (%)                  | 2.0            | 0.13         | 0.053        |

\*Errors are based on SD of triplicate measurements of scintillation counts and cell counts.

<sup>†</sup>Errors are provided by least-squares fits to data using Sigmaplot (SPSS).

<sup>‡</sup>Errors are derived using the general form:

$$\xi_x^2 = \left(\frac{\partial x}{\partial \mu_N}\right)^2 \xi_{\mu_N}^2 + \left(\frac{\partial x}{\partial \sigma}\right)^2 \xi_{\sigma}^2,$$

where  $\xi^2$  is variance.

It is of interest to compare the percentage of cells with zero tracks as predicted by the log normal distribution (i.e., <1 track) with the measured percentages of cells with zero tracks. Using the fitted values for the parameters μ<sub>N</sub> and σ, one can calculate the predicted number of cells with zero tracks at the maximum exposure time for any given dataset (i.e., 52 d, 4 d, and 1 d in Figs. 3A, 3B, and 3C, respectively) using the cumulative distribution function by substituting a<sub>o</sub> → N and μ<sub>a</sub> → μ<sub>N</sub> into Equation 10. Using this approach, the probability for the number of convolved tracks to be <1 is predicted to be 2.0%, 0.13%, and 0.053%, for experiments A, B, and C, respectively (Table 1, last row). The measured percentages of cells with zero tracks for the corresponding experiments were 14%, 3.4%, and

3.3% (Figs. 3A–3C, 0 tracks, filled bars). As mentioned in the Results, trypan blue exclusion measurements indicated that about 3% of the cells were nonviable and may not have taken up <sup>210</sup>Po-citrate. Subtraction of the 3% that corresponds to nonviable cells from the measured percentages of zero tracks yields corrected values of 11%, 0.4%, and 0.3%. The differences between the corrected and predicted values are likely to be related to the fact that latent images that form early in the exposure period are liable to fade during long exposure times, particularly in the presence of oxidizing agents and moisture. In fact, our data for the 52-d exposure had slightly more cells with zero tracks (14%) than did the data for the 26-d exposure (11%) (Fig. 3A). Incidentally, this argument coincides with an observation of

**TABLE 2**  
Fitted Parameters and Statistical Quantities for Log Normal Activity Distributions

| Parameter   | Value          |                |              |
|---|----------------|----------------|--------------|
|   | A              | B              | C            |
| Experiment  |                |                |              |
| Labeling concentration (kBq/mL)*                          | 0.52 ± 0.051   | 3.8 ± 0.36     | 67 ± 6.6     |
| Mean cellular activity <a <sub>o</sub> > (mBq/cell)*      | 0.054 ± 0.0037 | 0.12 ± 0.011   | 1.8 ± 0.22   |
| Scale parameter (μ <sub>a</sub> ) <sup>†</sup>            | −3.2 ± 0.11    | −2.3 ± 0.028   | 0.43 ± 0.029 |
| Shape parameter (σ) <sup>†</sup>                          | 0.80 ± 0.056   | 0.59 ± 0.023   | 0.52 ± 0.026 |
| Arithmetic mean (a <sub>o</sub> ) (mBq/cell) <sup>‡</sup> | 0.054 ± 0.0066 | 0.12 ± 0.0041  | 1.8 ± 0.062  |
| Median (mBq/cell) <sup>‡</sup>                            | 0.039 ± 0.0041 | 0.11 ± 0.0029  | 1.5 ± 0.046  |
| Mode (mBq/cell) <sup>‡</sup>                              | 0.021 ± 0.0032 | 0.074 ± 0.0029 | 1.2 ± 0.047  |

<sup>††</sup>Errors are obtained as described in Table 1.

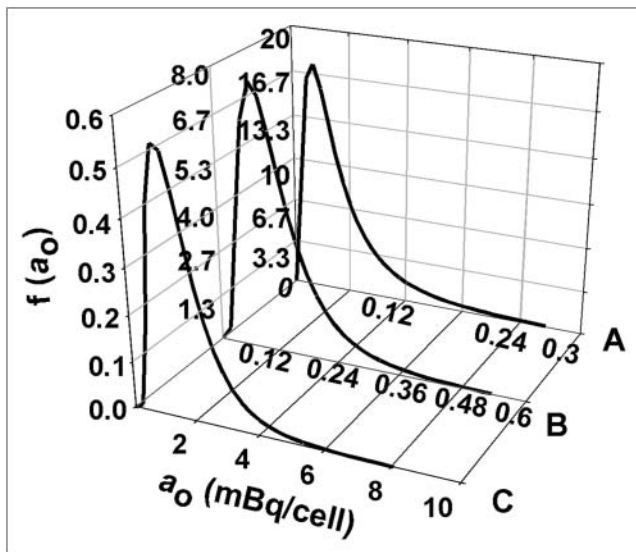


**FIGURE 5.** Log normal probability density function  $f(a_0)$  vs. initial cellular activity  $a_0$  for 3 different mean cellular activities  $\langle a_0 \rangle$ : 0.054 mBq per cell (A), 0.12 mBq per cell (B), 1.8 mBq per cell (C). Probability density functions were obtained using Equation 9 and parameters  $\mu_a$  and  $\sigma$  from Table 2.

Yagoda and Kaplan (17), who showed that when development of the emulsion was delayed for 10 d, the track count was reduced by 9.2%. They attributed this to partial fading of the older tracks (17). With these considerations in mind, our predicted and experimental percentages of cells with zero tracks are in good agreement. However, this statement should be tempered by the fact that the dark background of the emulsion precluded correlating zero track cells with trypan blue-positive cells.

It is evident from Figure 5 that, for  $^{210}\text{Po}$ -citrate, the shape of the log normal probability density function is essentially the same regardless of the mean initial activity per cell  $\langle a_0 \rangle$ . Furthermore,  $\langle a_0 \rangle$  is linearly dependent on the concentration of  $^{210}\text{Po}$ -citrate to which the cells are exposed in the present study (Fig. 1). Therefore, it is important to recognize the impact that the magnitude of  $\langle a_0 \rangle$  has on the log normal probability density function. Figure 5 shows how the probability density functions change when the mean activity per cell  $\langle a_0 \rangle$  is increased (i.e., expose the cells to correspondingly higher concentrations of extracellular activity). The shape parameter is similar in each case (Table 2); however, the scale parameter  $\mu_a$  depends on the mean cellular activity  $\langle a_0 \rangle$  according to Equation 11. In fact, it can be shown that if the mean activity is increased by an order of magnitude, the corresponding values of  $f(a_0)$  scale down by the same order of magnitude while the shape of the function remains the same.

Given that the activity per cell can vary widely even when a clonal population of cells is identically exposed to a radiochemical, then, depending on the geometry of the cell population, the cellular absorbed doses may also vary similarly. Numerous studies have been performed that examine

the implications of nonuniform distributions of radioactivity from the perspectives of both cellular dosimetry and microdosimetry (8,11,14,28,29). Although specific consideration of both labeled and unlabeled cells was considered, the paucity of experimental data on distribution of activity per cell required the assumption that the activity per cell among the labeled cells is constant. Accordingly, little attention has been devoted to the implications of variations in cellular uptake of radioactivity within the labeled population of cells. The present data, which quantitatively describe the nonuniform distribution of activity among a clonal population of cells, can be used to study the impact of such a distribution on the biologic response of a cell population. To focus solely on the impact of activity distribution, the stochastic nature of energy deposition by individual intracellular decays will be ignored. With this assumption, and assuming that the cells are sufficiently far from one another for there to be no cross-irradiation, then the mean cellular absorbed dose in a given cell is directly proportional to its initial cellular activity. Therefore, for radionuclides that emit high-LET (linear energy transfer)-type radiations, the fraction of surviving cells  $SF$  can be expressed as:

$$SF = \int_0^{\infty} f(a_0) e^{-a_0/a_{37}} da_0, \quad \text{Eq. 13}$$

where  $a_{37}$  is the mean lethal cellular activity. When assessing the lethality of incorporated radioactivity in cultured cells, the surviving fraction is generally measured as a function of the experimentally determined mean cellular activity  $\langle a_0 \rangle$  (30). Substitution of Equation 12 into Equation 13 gives the surviving fraction of the cell population  $SF$  containing a log normal distribution of activity with mean cellular activity  $\langle a_0 \rangle$ :

$$SF(\langle a_0 \rangle) = \int_0^{\infty} \frac{1}{a_0 \sigma \sqrt{2\pi}} e^{-(\ln a_0 - (\ln \langle a_0 \rangle - \sigma^2/2))^2 / 2\sigma^2} \times e^{-a_0/a_{37}} da_0. \quad \text{Eq. 14}$$

To examine the consequence of a log normal activity distribution on cell survival, a numeric integration of Equation 14 was performed with a simple FORTRAN code, wherein it was assumed that  $a_{37} = 0.13$  mBq per cell (23) and  $\sigma$  was varied from 0.4 to 1.0. For each value of  $\sigma$ , the survival fraction was calculated for numerous values of  $\langle a_0 \rangle$  and plotted in Figure 6. These data were compared with survival fractions obtained when each cell in the population contains the same activity—namely, the mean cellular activity  $\langle a_0 \rangle$  (i.e.,  $\sigma \rightarrow 0$  such that  $SF = \exp(-\langle a_0 \rangle/a_{37})$ ). It is apparent that the impact of the log normal distribution on the response of the cell population is dependent on the shape parameter  $\sigma$ . The shaded portion of the graph highlights the data generated with  $\sigma$  values corresponding to the range of the fitted  $\sigma$  values given in Table 1. Interestingly, this type of

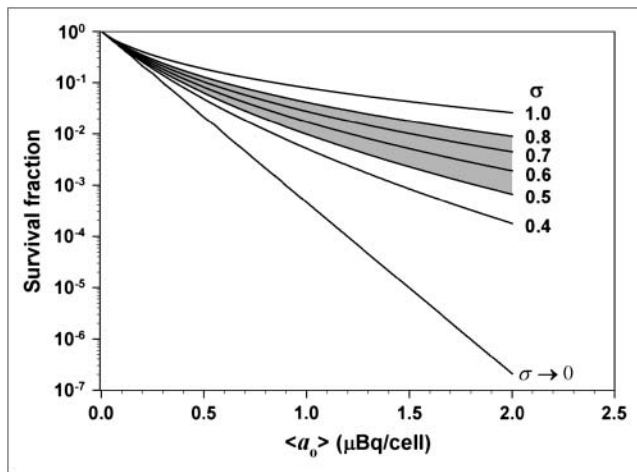


**FIGURE 6.** Calculated cell survival fraction (SF) vs. mean activity per cell  $\langle a_0 \rangle$  assuming a log normal distribution of activity per cell. Survival fractions were calculated for different values of  $\sigma$  according to Equation 14. Shaded region represents range of  $\sigma$  values that were observed for various  $^{210}\text{Po}$  activities used in the present studies. Condition  $\sigma \rightarrow 0$  represents the case where all cells in the population contain the same activity (i.e.,  $\text{SF} = \exp(-\langle a_0 \rangle / a_{37})$ ). Note profound impact that shape parameter  $\sigma$  has on survival curve.

tailing survival curve was not observed when V79 cells were exposed to  $^{210}\text{Po}$ -citrate (23); however, those experimental data included only 1 point below 10% survival. The log normal distribution does not have a profound effect on survival fractions above 10%. On the other hand, our recent studies with  $^{210}\text{Po}$ -citrate-labeled V79 cells in 3-dimensional cultures show significant tailing of survival curves (data not shown). Furthermore,  $^{131}\text{I}$ -iododeoxyuridine ( $^{131}\text{I}$ -IdU)-labeled V79 cells in 3-dimensional culture also show a similar tailing of the survival curve (21). Modeling calculations, which took into account the percentage of labeled cells and assumed equal activity per labeled cell, gave good agreement with the experimental data when the survival fraction exceeded 1% (31). However, the model did not predict the tail in the survival curve. There it was suggested that the distribution of cellular uptake of radioactivity may play an important role in modeling the response to  $^{131}\text{I}$ -IdU (31). The findings in the present work support this premise.

Although the present study highlights the importance of considering the distribution of cellular activity within a cell population when predicting biologic response, it should be pointed out that the mathematic nature of the distribution will determine its significance. For example, a very narrow distribution about the mean value might have little or no significant impact on the overall response of the population. Cellular uptake of Hoechst 33342, a flow cytometry dye for analyzing DNA content, often follows this pattern. However, log normal distributions are more likely the norm (27). Interestingly, most fluorescence cytometry reagents are best visualized under logarithmic amplification, thereby supporting this premise. Perhaps of more significance to nuclear medicine is the log normal uptake of PET radiopharmaceu-

tics in tumors (32). Nevertheless, the mathematic nature of the distribution will have to be determined experimentally for each radiopharmaceutical of interest. This will be important for radiopharmaceutical therapies in which targeting of single cells is necessary (33) as well as for micro-metastases and larger tumors (34).

Though differences in cellular uptake of radioactivity within a population are indeed important, as pointed out by others, there are numerous other factors that must be considered when predicting the response to incorporated radionuclides. Among them are the types of radiations emitted, dependence of relative biological effectiveness (RBE) on LET, differences in RBE for self- and cross-dose, presence of cells that do not take up any radioactivity at all, stochastic nature of the decay process, dose rate, and sub-cellular distribution of the radioactivity (14,15,31,35–38). In addition, care must be exercised if there is saturation in the uptake of radioactivity by tissues. Under these circumstances, it is possible that the probability distribution for cellular activity may be altered. This list is by no means exhaustive, thereby highlighting the complexity of the problem.

## CONCLUSION

The present study provides experimental evidence for a log normal distribution of cellular radioactivity within a cell population. The shape characteristics of the distribution remain the same as the mean activity is increased. Theoretic calculations show that the presence of a log normal activity distribution can have a profound impact on modeling the biologic response of cell populations.

## ACKNOWLEDGMENTS

This work was supported in part by U.S. Public Health Service grant R01CA83838. We are grateful to Drs. Edouard I. Azzam, Sonia de Toledo, Massimo Pinto, and Manuela Buonanno for their assistance.

## REFERENCES

1. Howell RW, Wessels BW, Loevinger R. The MIRD perspective 1999. *J Nucl Med.* 1999;40(suppl):3S–10S.
2. ICRU. ICRU Report No. 67. Absorbed-dose specification in nuclear medicine. *J ICRU.* 2002;2:3–110.
3. Humm JL. Dosimetric aspects of radiolabeled antibodies for tumor therapy. *J Nucl Med.* 1986;27:1490–1497.
4. Roesch WC. Microdosimetry of internal sources. *Radiat Res.* 1977;70:494–510.
5. Tisljar-Lentulis G, Feinendegen LE, Walther H. Calculation of specific energies of incorporated Pu-239 and I-131 in accordance with the concept of the critical cell. *Radiat Environ Biophys.* 1976;13:197–204.
6. Polig E. The localized dosimetry of internally deposited alpha-emitters. *Curr Top Radiat Res.* 1978;13:189–327.
7. Kozak RW, Atcher RW, Gansow OA, Friedman AM, Hines JJ, Waldmann TA. Bismuth-212-labeled anti-Tac monoclonal antibody: alpha-particle-emitting radionuclides as modalities for radioimmunotherapy. *Proc Natl Acad Sci U S A.* 1986;83:474–478.
8. Humm JL, Chin LM. A model of cell inactivation by alpha-particle internal emitters. *Radiat Res.* 1993;134:143–150.
9. Dadachova E, Howell RW, Bryan RA, Frenkel A, Nosanchuk JD, Casadevall A. Susceptibility of the human pathogenic fungi *Cryptococcus neoformans* and

- Histoplasma capsulatum to gamma-radiation versus radioimmunotherapy with alpha- and beta-emitting radioisotopes. *J Nucl Med.* 2004;45:313–320.
10. Walicka MA, Vaidyanathan G, Zalutsky MR, Adelstein SJ, Kassis AI. Survival and DNA damage in Chinese hamster V79 cells exposed to alpha particles emitted by DNA-incorporated astatine-211. *Radiat Res.* 1998;150:263–268.
  11. Roeske JC, Stinchcomb TG. The use of microdosimetric moments in evaluating cell survival for therapeutic alpha-particle emitters. *Radiat Res.* 1999;151:31–38.
  12. Charlton DE, Turner MS. Use of chord lengths through the nucleus to simulate the survival of mammalian cells exposed to high LET alpha-radiation. *Int J Radiat Biol.* 1996;69:213–217.
  13. Akabani G, Zalutsky MR. Microdosimetry of astatine-211 using histological images: application to bone marrow. *Radiat Res.* 1997;148:599–607.
  14. Goddu SM, Rao DV, Howell RW. Multicellular dosimetry for micrometastases: dependence of self-dose versus cross-dose to cell nuclei on type and energy of radiation and subcellular distribution of radionuclides. *J Nucl Med.* 1994;35:521–530.
  15. Faraggi M, Gardin I, Stievenart JL, Bok BD, Le Guludec D. Comparison of cellular and conventional dosimetry in assessing self-dose and cross-dose delivered to the cell nucleus by electron emissions of <sup>99m</sup>Tc, <sup>125</sup>I, <sup>111</sup>In, <sup>67</sup>Ga and <sup>201</sup>Tl. *Eur J Nucl Med.* 1998;25:205–214.
  16. Katz R, Pinkerton FE. Response of nuclear emulsions to ionizing radiations. *Nucl Inst Meth.* 1975;130:105–119.
  17. Yagoda H, Kaplan N. Quantitative alpha particle counting by the emulsion technique [letter]. *Phys Rev.* 1947;72:356.
  18. Erskine JR. Nuclear track emulsions. *Nucl Inst Meth.* 1979;162:371–378.
  19. Brooks AL, Benjamin SA, Hahn FF, Brownstein DG, Griffith WC, McClellan RO. The induction of liver tumors by <sup>239</sup>Pu citrate or <sup>239</sup>PuO<sub>2</sub> particles in the Chinese hamster. *Radiat Res.* 1983;96:135–151.
  20. Humm JL, Macklis RM, Bump K, Cobb LM, Chin LM. Internal dosimetry using data derived from autoradiographs. *J Nucl Med.* 1993;34:1811–1817.
  21. Neti PVS, Howell RW. When may a nonuniform distribution of <sup>131</sup>I be considered uniform? An experimental basis for multicellular dosimetry. *J Nucl Med.* 2003;44:2019–2026.
  22. Aitchison J, Brown JAC. *The Log-Normal Distribution.* Cambridge, U.K.: Cambridge University Press; 1957.
  23. Howell RW, Narra VR, Rao DV, Sastry KSR. Radiobiological effects of intracellular polonium-210 alpha emissions: a comparison with Auger-emitters. *Radiat Prot Dosimetry.* 1990;31:325–328.
  24. Gailar O, Seidlitz L, Bleuler E, Tendam DJ. Range-energy relations for alpha particles and deuterons in the Kodak NTB emulsion. *Rev Sci Instrum.* 1953;24:126–128.
  25. Ziegler JF. *TRIM, The Transport of Ions in Matter.* New York, NY: IBM; 1992.
  26. Fagerström T, Jagers P, Schuster P, Szathmary E. Biologists put on mathematical glasses. *Science.* 1996;274:2039–2040.
  27. Limpert E, Stahel WA, Abbt M. Log-normal distributions across the sciences: keys and clues. *Bioscience.* 2001;51:341–352.
  28. Roeske JC, Stinchcomb TG. Dosimetric framework for therapeutic alpha-particle emitters. *J Nucl Med.* 1997;38:1923–1928.
  29. Malaroda A, Flux G, Ott R. The application of dose-rate volume histograms and survival fractions to multicellular dosimetry. *Cancer Biother Radiopharm.* 2005;20:58–65.
  30. Kassis AI, Sastry KSR, Adelstein SJ. Kinetics of uptake, retention, and radiotoxicity of <sup>125</sup>IUDr in mammalian cells: implications of localized energy deposition by Auger processes. *Radiat Res.* 1987;109:78–89.
  31. Howell RW, Neti PV. Modeling multicellular response to nonuniform distributions of radioactivity: differences in cellular response to self-dose and cross-dose. *Radiat Res.* 2005;163:216–221.
  32. Thie JA, Hubner KF, Smith GT. The diagnostic utility of the lognormal behavior of PET standardized uptake values in tumors. *J Nucl Med.* 2000;41:1664–1672.
  33. McDevitt MR, Sgouros G, Finn RD, et al. Radioimmunotherapy with alpha-emitting nuclides. *Eur J Nucl Med.* 1998;25:1341–1351.
  34. Neti PVS, Howell RW. Isolating effects of microscopic nonuniform distributions of <sup>131</sup>I on labeled and unlabeled cells. *J Nucl Med.* 2004;45:1050–1058.
  35. Fisher DR. The microdosimetry of monoclonal antibodies labeled with alpha emitters. In: Schlafke-Stelson AT, Watson EE, eds. *Proceedings of Fourth International Radiopharmaceutical Dosimetry Symposium.* CONF-851113–(DE86010102). Springfield, VA: National Technical Information Service; 1986:26–36.
  36. Charlton DE, Sephton R. A relationship between microdosimetric spectra and cell survival for high-LET irradiation. *Int J Radiat Biol.* 1991;59:447–457.
  37. O'Donoghue JA, Wheldon TE. Dose-rate effects in biologically targeted radiotherapy. *Int J Radiat Biol.* 1989;56:745–749.
  38. Makrigiorgos GM, Ito S, Baranowska-Kortylewicz J, et al. Inhomogeneous deposition of radiopharmaceuticals at the cellular level: experimental evidence and dosimetric implications. *J Nucl Med.* 1990;31:1358–1363.